$Q_H^{\bullet-}$ Ubisemiquinone Radical in the bo_3-Type Ubiquinol Oxidase Studied by Pulsed Electron Paramagnetic Resonance and Hyperfine Sublevel Correlation Spectroscopy†

Stéphane Grimaldi,‡ Fraser MacMillan,*,‡ Thomas Ostermann,§,|| Bernd Ludwig,|| Hartmut Michel,§ and Thomas Prisner‡

Institut für Physikalische und Theoretische Chemie and Institut für Biochemie, J. W. Goethe Universität Frankfurt, D-60439 Frankfurt am Main, Germany, and Max-Planck-Institut für Biophysik, D-60528 Frankfurt am Main, Germany

Received July 13, 2000; Revised Manuscript Received October 6, 2000

ABSTRACT: The high-affinity Q_H ubiquinone-binding site in the bo_3 ubiquinol oxidase from *Escherichia coli* has been characterized by an investigation of the native ubiquinone radical anion $Q_H^{\bullet-}$ by pulsed electron paramagnetic resonance (EPR) spectroscopy. One- and two-dimensional electron spin−echo envelope modulation (ESEEM) spectra reveal strong interactions of the unpaired electron of $Q_H^{\bullet-}$ with a nitrogen nucleus from the surrounding protein matrix. From analysis of the experimental data, the ^{14}N nuclear quadrupolar parameters have been determined: $\kappa = e^2qQ/4h = 0.93$ MHz and $\eta = 0.50$. This assignment is confirmed by hyperfine sublevel correlation (HYSCORE) spectroscopy. On the basis of a comparison of these data with those obtained previously for other membrane-protein bound semiquinone radicals and model systems, this nucleus is assigned to a protein backbone nitrogen. This result is discussed with regard to the location and potential function of Q_H in the enzyme.

The bo_3 ubiquinol oxidase from *Escherichia coli* belongs to the heme−copper superfamily of respiratory oxidases that includes the mitochondrial cytochrome *c* oxidase (*1*). The bo_3 complex is a four-subunit enzyme (*2*) that contains three metal centers: a low-spin heme iron, a high-spin heme iron, and a copper center (Cu_B), all located in subunit I. The enzyme catalyzes the two-electron oxidation of ubiquinol 8 (UQ_8H_2) and the four-electron reduction of molecular oxygen to water in the cytoplasmic membrane (*3*), establishing an electrochemical proton gradient across the membrane not only via scalar protolytic reactions but also via a proton pump mechanism (*4*). Unlike cytochrome *c* oxidases, which contain a fourth redox metal center (Cu_A) accepting electrons from ferrocytochrome *c*, the oxidation of quinols by cytochrome bo_3 proceeds via the cooperation of one or two quinol/quinone binding sites whose location is still a matter of some debate: a low-affinity quinol oxidation site (labeled Q_L),[1] which is in dynamic equilibrium with the membrane quinone pool (*5*), and a high-affinity quinone binding site (labeled Q_H), which is proposed to mediate intramolecular electron transfer (*6*). It has been shown that, although cooperation of two quinone/quinol binding sites is crucial for the oxidation of substrates by quinol oxidases, the Q_L and Q_H sites of the bo_3 quinol oxidase are distinct from the Q_A and Q_B sites of the photosynthetic reaction center and the Q_o and Q_i sites of the cytochrome bc_1 complex in terms of substrate specificity, binding affinity, and redox properties (*5*, *6*).

Quinone binding sites, which are present in most biological respiratory and photosynthetic electron-transfer chains, are known to be able to modulate electron and proton transfer chemistry to an extent that very different quinone properties are associated with different binding sites. Therefore, they have been extensively studied by molecular biology and biophysical methods in order to identify and classify them.

The X-ray structure of the bacterial bo_3 complex has been solved recently, but no quinones were bound in the crystal form (*7*). A tentative assessment has been made to try and identify one putative Q_H site in subunit I, which has led to the determination of a key histidine residue contact. This has also been suggested by site-directed mutagenesis studies (see discussion in ref *8*). A reasonably well conserved sequence motif L-$(X)_3$-H-$(X)_3$-I triad in cytochrome *bo* sequences has been identified at this site, which might suggest a possible similarity with the Q_A and Q_B sites of bacterial reaction centers, the Q_i site of the mitochondrial

† This work was supported by the Deutsche Forschungsgemeinschaft (Sfb 472).

* Corresponding author: fax +49 69 79829404; e-mail fm@masklin.anorg.chemie.uni-frankfurt.de.

‡ Institut für Physikalische und Theoretische Chemie, J. W. Goethe Universität Frankfurt.

§ Max-Planck-Institut für Biophysik.

|| Institut für Biochemie, J. W. Goethe Universität Frankfurt.

[1] Abbreviations: A_1, phylloquinone in photosystem I; A_{iso}, isotropic hyperfine coupling; bRC, bacterial reaction centre; cw, continuous wave; DM, *n*-dodecyl-β-D-maltoside; DPPH, (α,α′)-diphenyl-β-picrylhydrazyl; EPR, electron paramagnetic resonance spectroscopy; ENDOR, electron nuclear double resonance spectroscopy; ESEEM, electron spin−echo envelope modulation spectroscopy; hfc, hyperfine couplings constants; HYSCORE, hyperfine sublevel correlation spectroscopy; MES, 2-(*N*-morpholino)ethanesulfonic acid; PSI, photosystem I; PSII, photosystem II; Q_A and Q_B, primary and secondary stable electron acceptors in type II reaction centres; Q_H, high-affinity ubiquinone-binding site of quinol oxidase; Q_L, low-affinity ubiquinol oxidation site of quinol oxidase; Q_0 and Q_i, quinones of the cytochrome bc_1 complex; TWT, traveling wave tube amplifier; UQ, ubiquinone; β_e, Bohr magneton; β_N, nuclear spin magneton.

10.1021/bi001641+ CCC: $20.00
Published on Web 01/06/2001

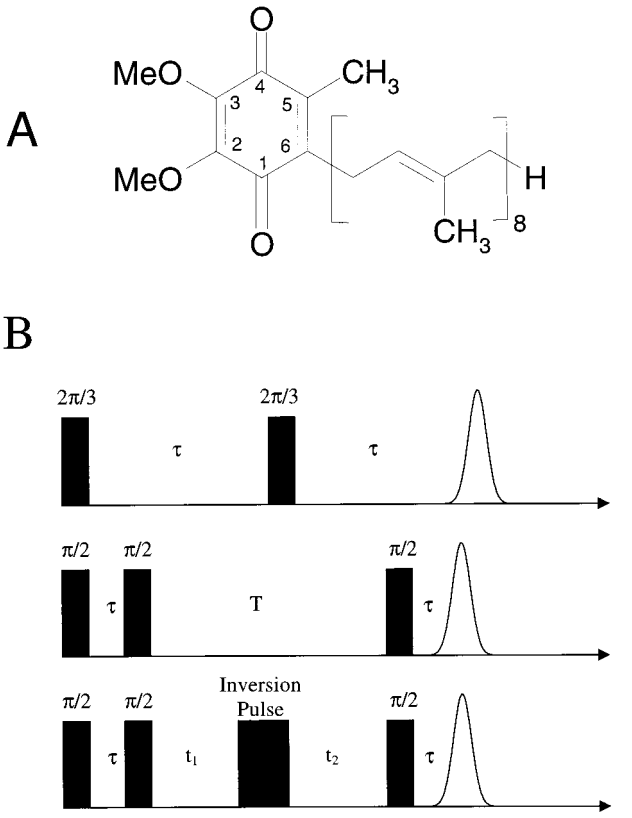

FIGURE 1: (A) Molecular structure and numbering scheme of ubiquinone 8 (Q_H). (B) Pulse sequences used in this work. From top to bottom: field-swept experiment, three-pulse ESEEM, and HYSCORE.

bc_1 complex, and maybe the phylloquinone sites in PSI as well as the ubiquinone binding sites in complex I (*8*).

The Q_H site studied in this work highly stabilizes the ubiquinone radical anion $Q_H^{\bullet -}$ (*9*, *10*). Unlike the weakly bound, low-affinity ubiquinone, the strongly bound, high-affinity ubiquinone is retained during enzyme preparation (*11*). The ubisemiquinone radical stabilized in the Q_H site of the purified *E. coli* bo_3-type ubiquinol oxidase has been previously studied by X-band (9 GHz) continuous wave (cw) electron paramagnetic resonance (EPR) (*9*, *10*) and Q-band (35 GHz) cw electron nuclear double resonance (ENDOR) spectroscopy (*12*). The cw X-band EPR spectrum exhibits a partially resolved hyperfine splitting indicative of a magnetic interaction. Very recently, numerical simulations of cw-EPR spectra recorded at 35 GHz (*12*), in comparison with studies performed on A_1 in PSI (*13*, *14*) led to the interpretation that this splitting results from the magnetic coupling of the three equivalent β-methyl protons at position 5 (see Figure 1A for molecular structure of Q_H). A comparison of samples in protonated and deuterated environments provided an indication for exchangeable protons, consistent with $Q_H^{\bullet -}$ being hydrogen-bonded to its protein surroundings, probably through one or both of its carbonyl oxygens.

The electron spin−echo envelope modulation (ESEEM) technique has been extensively used to study and provide detailed information related to the interactions of protein-bound quinone radicals with their immediate environment, as for example in bacterial reaction centers (*15*−*17*), photosystem I (*18*), and photosystem II (e.g., ref *19*). Thus an accurate estimation of weak nuclear hyperfine couplings, even in powder spectra, can be achieved. In favorable circumstances, the identity of the interacting nuclei and their chemical environment can also be determined.

To further investigate its coordination and the environment of the binding site, we report here the first ESEEM study of the $Q_H^{\bullet -}$ radical anion in bo_3 ubiquinol oxidase from *E. coli*. We apply the two-dimensional hyperfine sublevel correlation (HYSCORE) spectroscopy, which is a well-established method for elucidating the hyperfine couplings by providing correlations between nuclear frequencies originating from different m_s manifolds (*20*).

MATERIALS AND METHODS

Sample Preparation. The *E. coli* strain GO105/pJRHisA (*21*) was grown at 37 °C in LB medium containing 0.3% lactic acid and 100 μg/mL ampicilin in 5 L shaker flasks filled with 2 L of medium. Cells were harvested at mid-logarithmic phase with a continuous-flow centrifuge (Carl Padberg Zentrifugenbau GmbH, Lahr/Schwarzwald). The harvested cells were immediately resuspended in 50 mM K_2HPO_4 (pH 8), 100 mM NaCl, and 100 μM Pefabloc SC (Biomol) (25 mL of buffer/10 g of cells) and broken by passing through a microfluidizer (Microfluidics Corp., Newton Massachusetts) at 1000 bar on ice (3 times). Cell debris was removed by low-speed centrifugation (16000*g* for 10 min) and membranes were isolated from the supernatant by centrifugation at 200000*g* for 45 min. Membranes (with a protein concentration of 20 mg/mL) were then suspended in 50 mM K_2HPO_4 (pH 8) and solubilized with 2% DM (Calbiochem). The suspension was stirred at 4 °C for 30 min, centrifuged at 50000*g* for 10 min, and filtered through a 1.2 μm filter.

The bo_3 quinol oxidase was purified as described previously (*22*). Buffer exchange was performed on a small desalting column (PD-10 Sephadex G-25 M, Pharmacia). A buffer of 0.1 M MES, pH 6 or pH^* 6 (in D_2O, pH^* corresponds to pH-meter reading, $pD \approx pH^* + 0.4$), and 0.02% DM was used as an exchanging buffer. The deuterated samples were additionally diluted (1:100) in 0.1 M MES (pH* 6) and 0.01% DM. The enzyme was concentrated by ultrafiltration on a Biomax-30 filter (Millipore) up to final concentrations of ≈600 μM.

The reduction of bound quinone was performed under an argon atmosphere with a 500-fold excess of sodium ascorbate. The reduced sample in an argon-flushed EPR sample tube was immediately frozen in liquid nitrogen.

EPR Spectroscopy. X-Band cw-EPR spectra were recorded on a Bruker ESP300 spectrometer with a standard rectangular Bruker EPR cavity (ER4102T). Q-Band cw-EPR spectra were measured on a Bruker E-500 spectrometer with a standard Bruker resonator (ER 5106QT-W1). Both instruments were equipped with Oxford helium cryostats (ESR900 and CF935, respectively). The microwave frequency was measured by use of a Systron Donner (6054D) (X-band) and a Hewlett-Packard HP5352b (Q-band) frequency counter. The magnetic field was measured with a Bruker gaussmeter (ER035M). The measured *g*-values were corrected for an offset against a known *g* standard (DPPH with $g = 2.00351$).

X-Band pulsed EPR measurements were performed on a Bruker E-580 spectrometer with a standard dielectric resonator (MD5 W1) equipped with an Oxford helium (CF935) cryostat. The microwave pulses were amplified with a 20 W cw-TWT (Hughes). The field-swept spectrum was ob-

tained by integrating the two-pulse echo signal as a function of the magnetic field after a two-pulse sequence (Figure 1B).

In three-pulse ESEEM spectroscopy (Figure 1B), the amplitude of the stimulated echo as a function of τ and T was measured at a frequency of approximately 9.6 GHz, at a magnetic field corresponding to the maximum intensity of the field-swept spectrum where all orientations of the molecule with respect to the magnetic field contribute. The minimum pulse separation time T was 192 ns and was incremented in steps of 8 ns (1024 data points); the duration of the $\pi/2$ pulse was 48 ns. Measurements were carried out at 20 K and τ values were varied from 192 to 344 ns in order to avoid suppression effects (*23*).

2D HYSCORE spectra were recorded, where the echo amplitude is measured as a function of t_1 and t_2 (Figure 1B) (*20*). The durations of the $\pi/2$ and inversion pulses were 48 and 68 ns, respectively, with equal amplitudes. A set of 512 $\times$ 512 data points was recorded. t_1 and t_2 were incremented in steps of 20 ns from their initial values.

To remove the unwanted echoes, the appropriate four-step phase-cycling procedures in the stimulated echo (*24*) and HYSCORE (*25*) experiments were applied.

THEORY

The Hamilton operator describing the magnetic interaction between an electron spin $S = 1/2$ (ubisemiquinone radical, for example) and a nitrogen nucleus (nuclear spin $I = 1$) can be described in the high-field approximation by

$$H = g_{\text{eff}}\beta_e B_0 S_Z - g_N\beta_N B_0 I_Z + \vec{S}\tilde{A}\vec{I} + \vec{I}\tilde{P}\vec{I} \qquad (1)$$

where g_{eff} is the effective g-value and B_0 is the external magnetic field, assumed to be directed along the z-direction. The second term in the Hamiltonian describes the Zeeman interaction of the nuclear spin I with B_0. The hyperfine coupling tensor $\tilde{\mathbf{A}}$ consists of the isotropic contribution A_{iso} and the traceless tensor $\tilde{\mathbf{T}}$ describing the anisotropic hyperfine coupling. The nuclear quadrupole interaction tensor $\tilde{\mathbf{P}}$ [with its principal values (V_{XX}, V_{YY}, V_{ZZ})] is traceless by definition. In its principal axis system the final term in eq 1 is expressed in the form

$$\vec{I}\tilde{\mathbf{P}}\vec{I} = \kappa[3I_Z^2 - I^2 + \eta(I_X^2 - I_Y^2)] \qquad (2)$$

where κ represents the quadrupole coupling constant $e^2qQ/4h$, $\eta = |(V_{XX} - V_{YY})/V_{ZZ}|$ is the asymmetry parameter of the electric field gradient on the nucleus, e is the elementary charge, Q is the nuclear quadrupole moment, and h is Planck's constant.

RESULTS

Figure 2 shows the cw X-band (A, B) and Q-band EPR spectra (C, D) of the ubisemiquinone radical $Q_H^{\bullet-}$ from the bo_3 ubiquinol oxidase from *E. coli* under nonsaturating conditions. The EPR signal has a line width of approximately 9.7 G at X-band and exhibits a partially resolved hyperfine structure in the low-field region of the spectrum. Replacement of the buffer with D_2O-exchanged buffer alters the line shape of the spectrum, increasing the resolution of the splitting in the low-field region and shifting the minimum of the high-field region to a lower field value (Figure 2B). This would indicate the presence of exchangeable protons

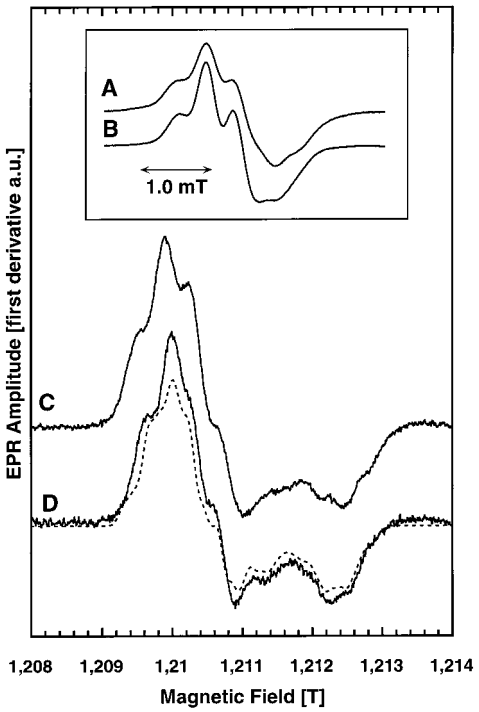

FIGURE 2: X-band and Q-band cw-EPR spectra of $Q_H^{\bullet-}$ in protonated (A, C) and deuterated (B, D) buffer. Experimental conditions: (A, B) microwave power 0.1 mW, field modulation frequency 100 kHz, field modulation depth 0.5 G, temperature 80 K; (C) microwave power 0.6 μW, field modulation depth 2 G, temperature 80 K; (D) microwave power 1.2 μW, field modulation depth 2 G, temperature 80 K. The simulation of the Q-band (34.01 GHz) EPR powder spectrum (D) is shown as dotted lines. Parameters used were $g_{xx} = 2.00605$, $g_{yy} = 2.00519$, and $g_{zz} = 2.00213$ ($\pm$ 0.0001). Three equivalent protons have the following hyperfine tensor: $A_{xx} = 7.85$, $A_{yy} = 12.78$, and $A_{zz} = 8.40$ MHz; A_{zz} is parallel to g_{zz} and $\phi = 27°$ where ϕ is the angle between the $\tilde{\mathbf{g}}$ and $\tilde{\mathbf{A}}$ tensors.

close by or directly coordinated to the quinone radical (e.g., hydrogen bonds).

To determine the g-values of the radical, we have also performed Q-band measurements and carried out spectral simulations of the radical in deuterated buffer. The simulation is shown as dotted lines in Figure 2D. The $\tilde{\mathbf{g}}$ tensor (see figure caption) determined from numerical simulations is similar to that seen in other protein-bound $UQ^{\bullet-}$ anion radicals (*26*). It has been clearly demonstrated by high-field EPR (*27*) that the position of the g_{xx} component is very sensitive to the electrostatic environment around the semiquinone. The values determined for $Q_A^{\bullet-}$ and $Q_B^{\bullet-}$ in bacterial reaction centers (*28*) demonstrate this sensitivity for two identical radicals in differing protein environments. The values determined by Veselov et al. (*12*) have a similar anisotropy (as given by $g_{xx} - g_{zz}$) to those observed here; however, the absolute values are different. Taking the absolute value observed here and comparing with published data (*29*) clearly indicates hydrogen bonding (*27*). Further, we have also determined the angle between the $\tilde{\mathbf{g}}$ tensor and the proton methyl tensor at position 5 (see Figure 1). This angle of 27° also indicates the influence of hydrogen bonding to the neighboring carbonyl group, as has been shown previously (*27*).

To study the direct environment of the ubiquinone molecule in the Q_H site, we have performed X-band three-pulse ESEEM spectroscopy at a static magnetic field $B_0 =$

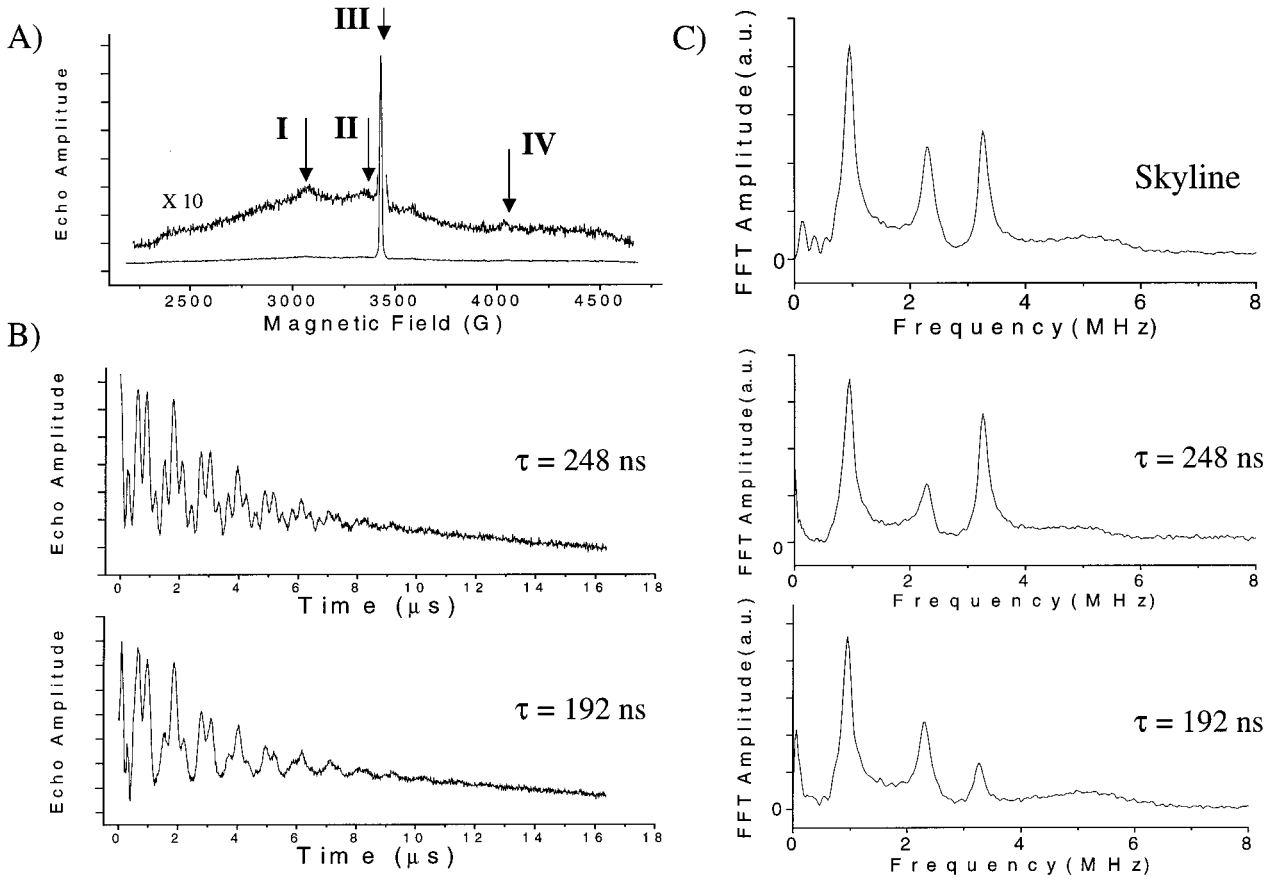

FIGURE 3: (A) Field-swept spectrum recorded at 20 K. Experimental conditions: pulse lengths, 48 ns; τ-value, 208 ns; shot repetition time, 2 ms; field sweep width, 2800 G; center field, 3431 G. Also shown are time-domain three-pulse ESEEM spectra (B) and Fourier transform (C, absolute value mode) of $Q_H^{\bullet -}$ recorded at two different τ-values. Experimental conditions: $\pi/2$ pulse length, 48 ns; temperature, 20 K; center field. 3430 G; microwave frequency, 9.64 GHz. A background correction with a fourth-order polynomial function has been used to remove the decay of the echo amplitude due to relaxation processes, followed by zero-filling to 2048 points and tapering with a Hamming function. The skyline spectrum corresponds to the skyline projection of three-pulse ESEEM spectra recorded at 20 τ values from 192 ns in steps of 8 ns.

343.0 mT corresponding to the maximum intensity of the echo-detected field-swept spectrum (see Figure 3A, position III); the ^{14}N Larmor frequency for this field is $\nu_I = 1.06$ MHz. Figure 3B displays two stimulated-echo decay spectra in the time domain for two different τ values (192 and 248 ns). The corresponding frequency-domain spectra are depicted in Figure 3C. The top trace in Figure 3C is a "suppression-free" spectrum, which is the skyline projection of the Fourier transform of the stimulated echo ESEEM spectra recorded at 20 τ values (from 192 to 344 ns in 8 ns steps). Four frequency components are clearly resolved: three narrow lines with peaks at 0.95, 2.32, and 3.27 MHz and a broad line with a maximum at ~5.2 MHz. A characteristic proton matrix peak appearing at about 14.8−15 MHz is also present in the spectra but will not be considered further in the following (data not shown).

The simple additive relationship satisfied by three of the four peaks observed (the sum of the 0.95 and 2.32 MHz frequencies equalling the 3.27 MHz frequency) and their typical profile allow us to assign them to ^{14}N ($I = 1$) nuclear transitions in the case where the so-called "cancellation condition" (*30*) is fulfilled; that is to say, when the nuclear Zeeman and hyperfine splitting effectively cancel in one electron-spin manifold (i.e., $A/2 = \nu_I$). In this manifold, the nuclear spin Hamiltonian reduces to the purely quadrupole Hamiltonian and the nitrogen nuclear quadrupolar resonance (NQR) transitions observed (the three narrow, low-frequency components) are given by the relationships

$$\nu_0 = 2\kappa\eta \qquad \nu_- = \kappa(3-\eta) \qquad \nu_+ = \kappa(3+\eta) \quad (3)$$

where κ represents the quadrupole coupling constant and η is the asymmetry parameter of the electric field gradient on the nucleus. The cancellation condition of the effective field prevents any frequency dispersion related to the orientation of B_0, so that these lines reveal no anisotropic broadening, leading to a sharp profile, while a moderate deviation from the exact cancellation would drastically reduce the intensities of the observed peaks whereas their positions would remain almost constant.

The hyperfine manifold, where the nuclear−Zeeman and the hyperfine interactions are additive, gives rise to much broader resonances (*30*) and the only resolvable component is a double quantum transition line, $\Delta m_I = 2$, occurring at higher frequencies. This line has maximum intensity at a frequency that is approximated by

$$\nu_{dq\pm} \approx 2[(\nu_I \pm A/2)^2 + \kappa^2(3+\eta^2)]^{1/2} \quad (4)$$

where A is a secular component of the hyperfine coupling tensor determined mainly from its isotropic part in the case of a small anisotropic hyperfine tensor; a modest anisotropy

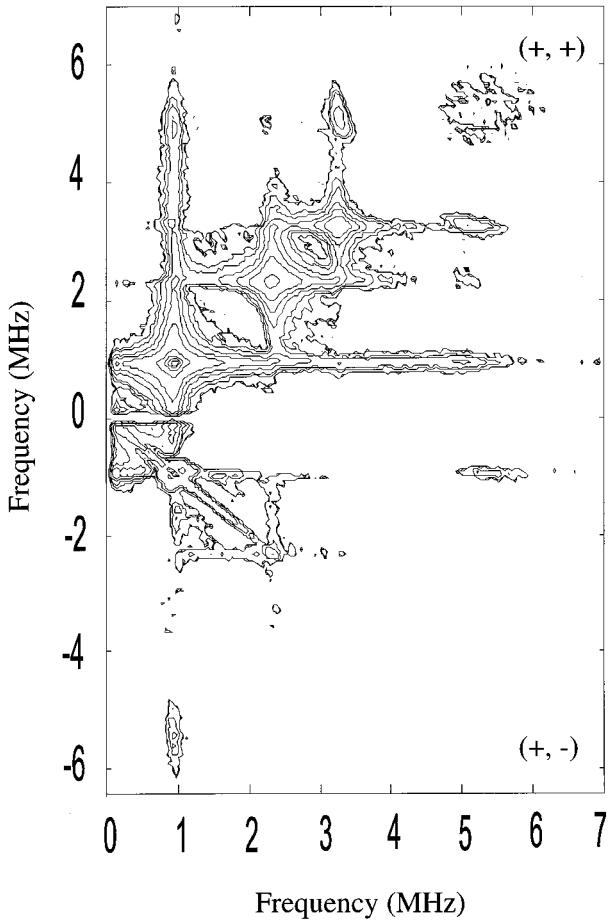

FIGURE 4: Experimental 2D HYSCORE spectrum (contour plots, absolute value mode) of $Q_H^{\bullet-}$ recorded with $\tau = 192$ ns; temperature, 20 K; center field, 3433 G; microwave frequency, 9.64 GHz. The background decay in both t_1 and t_2 dimensions was subtracted by use of a polynomial function followed by zero-filling to 1024 points in both dimensions and tapering with a Hamming window, before Fourier transformation.

of the hyperfine interaction affects mainly the line shape but not the frequency of this double quantum line (*30*).

The application of eq 3 to the three lines at 0.95, 2.32, and 3.27 MHz, assigned respectively to ν_0, ν_-, and ν_+, gives $\kappa = 0.93$ MHz and $\eta = 0.50$. From eq 4, the assignment of $\nu_{dq\pm} = 5.2$ MHz leads to a value of $A_{iso} = 1.8 \pm 0.4$ MHz. Although this estimated A value deviates from the $2\nu_I$ value (i.e., $|A_{iso} - 2\nu_I| = 0.4 \pm 0.4$ MHz), this deviation does not exceed $4\kappa/3 \approx 1.24$ MHz, which is the limiting value for the validity of the cancellation condition (*30*). The so-called "intermediate K regime" for which the K value is close to the value of $A/2$ has been shown to be characterized by the absence of single quantum peaks in the second M_s manifold and a broadening of the double quantum peak (*30*) in the case of a powder spectrum, which is in accordance with that observed in our spectra.

The above theoretical analysis is strongly indicative for the interpretation of the data, but in order to confirm this and to ensure that the observed peaks originate from only one nitrogen nucleus, we have performed 2D HYSCORE experiments (Figure 4). The 2D HYSCORE spectra exhibit only cross-peaks between hyperfine frequencies belonging to different M_s manifolds of the same nucleus (*20*). Therefore, peaks at (ν_{dq},ν_0), (ν_{dq},ν_-), and (ν_{dq},ν_+) are expected. The 2D HYSCORE spectrum of $Q_H^{\bullet-}$, recorded at the resonant magnetic field at which the echo amplitude reaches maximum, is presented as a contour plot in Figure 4. The on-diagonal features in both quadrants have a dominant intensity. They are due to weak field strength of the inversion pulse (*25*). The off-diagonal features are quite symmetrical with respect to the diagonals in both quadrants, and this agrees well with the theory (*31*). The spectrum exhibits an intense cross-peak at [5.2 (ν_{dq}), 3.3 (ν_+)] and two weaker cross-peaks at [5.2 (ν_{dq}), 2.3 (ν_-)] and [5.2 (ν_{dq}), 0.9 (ν_0)] MHz. This particular difference in cross-peak intensity is in accordance with previous HYSCORE studies leading to the observation that, as compared to the correlation peaks at $[\nu_0,\nu_{dq}]$ and $[\nu_-,\nu_{dq}]$, those at $[\nu_+,\nu_{dq}]$ are more intense and are most easily detected in experimental ^{14}N HYSCORE spectra (e.g., ref *32*). The appearance of these cross-peaks provides an unambiguous assignment of the 5.2 MHz peak to ν_{dq} and not to a nuclear transition frequency of a second nitrogen nucleus.

To ensure that some of the observed ESEEM modulations do not arise from the low-spin heme *b*, whose spectrum overlaps with that of the quinone, we have also performed ESEEM at different field positions (Figure 3A, arrows I, II, and IV). Despite a worse signal-to-noise ratio, the observed modulations were clearly different than those presented in Figure 3 (data not shown), confirming that the observed nitrogen nucleus is interacting with the $Q_H^{\bullet-}$ semiquinone radical.

DISCUSSION

The Q_H site is known to bind quinone much more tightly than the Q_L site, whose quinone may exchange with the ubiquinone pool (*5*). Unlike the Q_o and Q_i sites of the cytochrome bc_1 complex and the Q_B site of the photosynthetic RC, the Q_H site appears not to be in dynamic equilibrium with this membrane quinone pool (*5*). The conditions that have been used for our study served to remove weakly bound ubiquinone but to leave the strongly bound ubiquinone at this high-affinity center. X- and Q-band cw-EPR spectra presented a characteristic ubisemiquinone signal with an average g-value of 2.00425 ($\pm$0.0001). This value is similar to those reported previously for ubisemiquinone anion in quinol oxidase, in photosynthetic reaction centers, and in polar solvents (*12*, *26*−*29*).

Replacement of protonated buffer with deuterated buffer leads to a modification of the line shape of the observed EPR signal, suggesting the presence of exchangeable protons (hydrogen bonds) to the quinone, as has been recently observed (*12*).

ESEEM spectroscopy carried out on the stabilized $Q_H^{\bullet-}$ radical exhibited strong ESEEM modulations. By use of two-dimensional HYSCORE spectroscopy, this signal has been assigned to one nitrogen nucleus with quadrupolar parameters $\kappa = 0.93$ MHz and $\eta = 0.50$ directly interacting with the ubiquinone radical where the case of "cancellation condition" is fulfilled.

Although it is not possible to identify the origin of the nitrogen solely by means of the ESEEM data, useful indications are obtained by comparison of the ^{14}N nuclear quadrupolar parameters (κ, η) calculated from the present ESEEM data with nuclear quadrupole resonance (NQR) data available from the literature. The values for κ and η found

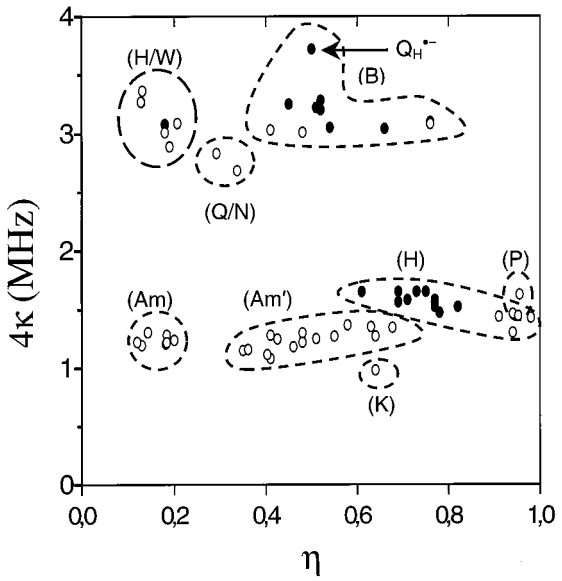

FIGURE 5: Two-dimensional plot of quadrupolar parameters of interacting nitrogens as obtained by ^{14}N-ESEEM spectroscopy of quinones in different membrane proteins (●) and by ^{14}N-NQR on model systems (○) (see ref *33* and references therein for ^{14}N-NQR data). (H/W) Indole, tryptophan, and histidine N(ϵ) nitrogen, *18*; (Q/N) glutamine and asparagine NH_2 nitrogen; (B) backbone nitrogen, peptide, di- and tripeptide, triglycine, *16*, *17*, *19*; (Am) and (Am′) NH_3^+ amino group nitrogen, (K) NH_3^+ lysine nitrogen, (P) proline nitrogen, (H) and histidine N(δ) nitrogen, *16*, *17*, *19*.

in our work seem to be nearly identical to those found in NQR studies of the peptide nitrogens in small di- and tripeptides (*33*) and to the reported cases of ESEEM data arising from the modulation of an amide nitrogen of the peptide backbone in respiratory and in photosynthetic protein complexes (*15*−*19*; see Figure 5). Comparison with these values shows that the nitrogen interacting here with the ubiquinone radical in the $Q_H^{\bullet-}$ site is most likely to correspond to an amide group of the protein backbone, very similar to the situation in $Q_A^{\bullet-}$ in PSII or in bRC (see Figure 5). It is also interesting to note that, at present, no histidine nitrogen, whose quadrupolar parameters have been well-characterized in other quinone binding sites (e.g., also in $Q_A^{\bullet-}$ in bRCs) by ESEEM spectroscopy (*16*, *17*, *19*), is detected in the Q_H binding site, although it has been predicted by the classification study of known quinone binding sites (*8*) and from molecular modeling in the X-ray crystal structure (see discussion in ref *8*).

The large isotropic hyperfine coupling value between $Q_H^{\bullet-}$ and ^{14}N ($A_{iso} \approx 1.8$ MHz) demonstrates a delocalization of the electron spin density of $Q_H^{\bullet-}$ onto the nitrogen. This is much larger than a purely dipolar coupling estimated over a distance of 3−3.5 Å (<0.2 MHz), suggesting that spin density is directly transferred from the quinone anion radical to the amino acid nitrogen and would indicate the presence of a hydrogen bond between $Q_H^{\bullet-}$ and N at the O_4 or at the O_1 oxygen (see Figure 1A). The magnitude and orientation of the hyperfine coupling assigned to the methyl group at position 5 as compared to model systems would suggest, on the basis of a simple valence-bond model (*34*), that this hydrogen bond is probably formed to O_1. ^{1}H ENDOR spectroscopy of these samples directly detects the interaction of such a hydrogen bond (data not shown), giving results very similar to those already published (*12*). Performing ESEEM experiments in the pH range 6−8.5, we have not yet observed any other interacting nitrogen, suggesting either that the hydrogen-bond donor at the other end of the quinone molecule is not a magnetic nucleus, that the interaction is much weaker, or that the cancellation condition discussed above is not fulfilled for these nuclei.

CONCLUSION

The crystals of *bo*$_3$ ubiquinol oxidase that were used to solve the three-dimensional structure of the enzyme have no bound quinones (*7*). Until now no detailed studies about the location of Q_H have been provided. Here we demonstrate that it is anchored to the protein via a hydrogen bond to the amide backbone. In its paramagnetic state it appears, presently, not to be electronically coupled to either a histidine or a tryptophan. Both have been suggested in mutagenesis studies to play a role in its function (*9*, *35*). Recently a potential quinone-binding site has been modeled in the electron density map of the *bo*$_3$ ubiquinol oxidase from *E. coli* (*7*). If confirmed, this would imply a center-to-center distance of about 13 Å between the quinone and heme *b*. A very interesting experiment would be to perform a pulsed electron−electron double resonance experiment to measure directly the distance and orientation of $Q_H^{\bullet-}$ relative to heme *b* in a fashion similar to that performed previously on different radical species in photosystem II (e.g., ref *36*). This should lead to the localization of the Q_H binding site within subunit II and aid the crystallographers in their future structure models. Such experiments are currently being performed in our laboratory.

ACKNOWLEDGMENT

We thank Robert Fiege, Robert Bittl, and Wolfgang Lubitz (TU Berlin, Germany) for the use of their EPR simulation program and R. B. Gennis (Urbana, IL) for the kind gift of strain GO105 as well as plasmid pJRHisA. The Q-band EPR was performed at Bruker Analytik GmbH (Karlsruhe, Germany). The Deutsche Forschungsgemeinschaft (Sfb 472) is thanked for financial support.

REFERENCES

1. Garcia-Horsman, J. A., Barquera, B., Rumbley, J., Ma, J., and Gennis, R. B. (1994) *J. Bacteriol. 176*, 5587−5600.
2. Kranz, R. G., and Gennis, R. B. (1983) *J. Biol. Chem. 258*, 10614−10621.
3. Anraku, Y., and Gennis, R. B. (1987) *Trends. Biochem. Sci. 12*, 262−266.
4. Puustinen, A., Finel, M., Haltia, T., Gennis, R. B., and Wikström, M. (1991) *Biochemistry 30*, 3936−3942.
5. Sato-Watanabe, M., Mogi, T., Miyoshi, H., Iwamura, H., Matsushita, K., Adachi, O., and Anraku, Y. (1994) *J. Biol. Chem. 269*, 28899−28907.
6. Sato-Watanabe, M., Mogi, T., Ogura, T., Kitagawa, T., Miyoshi, H., Iwamura, H., and Anraku, Y. (1994) *J. Biol. Chem. 269*, 28908−28912.
7. Abramson, J., Riistama, S., Larsson, G., Jasaitis, A., Svensson-Ek, M., Laakkonen, L., Puustinen, A., Iwata, S., and Wikström, M. (2000) *Nat. Struct. Biol.* 7, 910−917.
8. Fisher, N., and Rich, P. R. (2000) *J. Mol. Biol. 296*, 1153−1162.
9. Ingledew, W. J., Ohnishi, T., and Salerno, J. C. (1995) *Eur. J. Biochem. 227*, 903−908.
10. Sato-Watanabe, M., Itoh, S., Mogi, T., Matsuura, K., Miyoshi, H., and Anraku, Y. (1995) *FEBS Lett. 374*, 265−269.

11. Puustinen, A., Verkhovsky, M. I., Morgan, J. E., Belevich, N. P., and Wikström, M. (1996) *Proc. Natl. Acad. Sci. U.S.A. 93*, 1545−1548.
12. Veselov, A. V., Osborne, J. P., Gennis, R. B., and Scholes, C. P. (2000) *Biochemistry 39*, 3169−3175.
13. Rigby, S. E. J., Evans, M. C. W., and Heathcote, P. (1996) *Biochemistry 35*, 6651−6656.
14. MacMillan, F., Hanley, J., van der Weerd, L., Knüpling, M., Un, S., and Rutherford, A. W. (1997) *Biochemistry 36*, 9297−9303.
15. Bosch, M. K., Gast, P., Hoff, A. J., Spoyalov, A. P., and Tsvetkov, Yu. D. (1995) *Chem. Phys. Lett. 239*, 306−312.
16. Lendzian, F., Rautter, J., Käss, H., Gardiner, A., and Lubitz, W. (1996) *Ber. Bunsen-Ges. Phys. Chem. 100*, 2036−2040.
17. Spoyalov, A. P., Hulsebosch, R. J., Shochat, S., Gast, P., and Hoff, A. (1996) *Chem. Phys. Lett. 263*, 715−720.
18. Hanley, J., Deligiannakis, Y., MacMillan, F., Bottin, H., and Rutherford, A. W. (1997) *Biochemistry 36*, 11543−11549.
19. Deligiannakis, Y., Hanley, J., and Rutherford, A. W. (1999) *J. Am. Chem. Soc. 121*, 7653−7664
20. Höfer, P., Grupp, A., Nebenführ, H., and Mehring, M. (1986) *Chem. Phys. Lett. 132*, 279−282.
21. Rumbley, J. N., Nickels, E. F., and Gennis, R. B. (1997) *Biochim. Biophys. Acta 1340*, 131−142.
22. Schröter, T., Winterstein, C., Ludwig, B., and Richter, O.-M. H. (1998) *FEBS Lett. 432*, 109−112.
23. Mims, W. B. (1972) *Phys. Rev. B6*, 3543−3545.
24. Fauth, J. M., Schweiger, A., Braunschweiler, L., Forrer, J., and Ernst, R. R. (1986) *J. Magn. Reson. 66*, 74−85.
25. Gemperle, G., Aebli, G., Schweiger, A., and Ernst, R. R. (1990) *J. Magn. Reson. 88*, 241−256.
26. Lubitz, W., and Feher, G. (1999) *Appl. Magn. Reson. 17*, 1−48.
27. Burghaus, O., Plato, M., Rohrer, M., Möbius, K., MacMillan, F., and Lubitz, W. (1993) *J. Phys. Chem. 97*, 7639−7647.
28. Isaccson, R. I., Lendzian, F., Abresch, E. C., Lubitz, W., and Feher, G. (1995) *Biophys. J. 69*, 311−322.
29. Nimz, O. Lendzian, F., Boullais, C., and Lubitz, W. (1998) *Appl. Magn. Res. 14*, 255−274.
30. Flanagan, H. L., and Singel, D. J. (1987) *J. Chem. Phys. 87*, 5606−5616.
31. Shane J. J., Höfer, P., Reijerse, E. J., and De Boer, E. (1992) *J. Magn. Reson. 99*, 596−604.
32. Kofman, V., Shane, J. J., Dikanov, S. A., Bowman, M. K., Libman, J., Shanzer, A., and Goldfarb, D. (1995*) J. Am. Chem. Soc. 117*, 12771−12778.
33. Edmonds, D. T. (1977) *Phys. Rep. C 29*, 233−290.
34. MacMillan, F., Lendzian, F., Renger, G., and Lubitz, W. (1995) *Biochemistry, 34*, 8144−8156.
35. Ma, J., Puustinen, A., Wikström, M., and Gennis, R. B. (1998) *Biochemistry 37*, 11806−11811.
36. Astashkin, A. V., Hara, H., and Kawamori, A. (1998) *J. Chem. Phys. 108*, 3805−3812.

BI001641+